Nonlinear Dynamics of Spinning Bosonic Stars: Formation and Stability

N. Sanchis-Gual,[1] F. Di Giovanni,[2] M. Zilhão,[1] C. Herdeiro,[1,3] P. Cerdá-Durán,[2] J. A. Font,[2,4] and E. Radu[3]
[1]Centro de Astrofísica e Gravitação—CENTRA, Departamento de Física, Instituto Superior Técnico—IST, Universidade de Lisboa—UL, Avenida Rovisco Pais 1, 1049-001 Lisboa, Portugal
[2]Departamento de Astronomía y Astrofísica, Universitat de València, Dr. Moliner 50, 46100 Burjassot (València), Spain
[3]Departamento de Matemática da Universidade de Aveiro and Centre for Research and Development in Mathematics and Applications (CIDMA), Campus de Santiago, 3810-183 Aveiro, Portugal
[4]Observatori Astronòmic, Universitat de València, C/ Catedrático José Beltrán 2, 46980 Paterna (València), Spain

(Received 4 August 2019; published 25 November 2019)

We perform numerical evolutions of the fully nonlinear Einstein (complex, massive) Klein-Gordon and Einstein (complex) Proca systems, to assess the formation and stability of spinning bosonic stars. In the scalar (vector) case these are known as boson (Proca) stars. Firstly, we consider the formation scenario. Starting with constraint-obeying initial data, describing a dilute, axisymmetric cloud of spinning scalar or Proca field, gravitational collapse toward a spinning star occurs, via gravitational cooling. In the scalar case the formation is transient, even for a nonperturbed initial cloud; a nonaxisymmetric instability always develops ejecting all the angular momentum from the scalar star. In the Proca case, by contrast, no instability is observed and the evolutions are compatible with the formation of a spinning Proca star. Secondly, we address the stability of an existing star, a stationary solution of the field equations. In the scalar case, a nonaxisymmetric perturbation develops, collapsing the star to a spinning black hole. No such instability is found in the Proca case, where the star survives large amplitude perturbations; moreover, some excited Proca stars decay to, and remain as, fundamental states. Our analysis suggests bosonic stars have different stability properties in the scalar (vector) case, which we tentatively relate to its toroidal (spheroidal) morphology. A parallelism with instabilities of spinning fluid stars is briefly discussed.

DOI: 10.1103/PhysRevLett.123.221101

Introduction.—Recent data from gravitational-wave astronomy [1], as well as from electromagnetic very large baseline interferometry observations near galactic centers [2,3], support the black hole (BH) hypothesis: BHs commonly populate the cosmos, with masses spanning a range of (at least) 10 orders of magnitude. Yet, the elusiveness of the event horizon, the defining property of a BH, rules out an observational "proof" of their existence. Considering, thus, models of BH mimickers is a valuable tool to understanding the uniqueness of BH phenomenology.

Within the landscape of BH mimickers, bosonic stars (BSs) are particularly well motivated. They arise in simple and physically sound field theoretical models: complex, massive, bosonic fields (scalar [4,5] or vector [6]) minimally coupled to Einstein's gravity. Dynamically, moreover, static, spherical BSs are viable; for some range of parameters, the lowest energy stars—the fundamental family (FF)—have a formation mechanism [7,8] and are perturbatively stable [6,9–11]. The properties and phenomenology of such static BSs have been considered at length (see, e.g., the reviews [12,13]), including dynamical situations such as orbiting binaries, from which gravitational waveforms have been extracted [14–16]. These studies unveiled a close parallel in the phenomenology of spherical BSs, regardless of their scalar or vector nature.

Astrophysically, however, rotation is ubiquitous and should, thus, be included in more realistic models of BSs. Both scalar [17–19] and vector [6,20] axisymmetric, spinning BSs (SBSs) have been constructed and some of their phenomenology has been studied [21,22]. Yet, their dynamical and stability properties, a key aspect of their physical viability, have remained essentially unexplored; see the discussion in Ref. [23].

In this Letter we describe the dynamical properties of SBSs, obtained from fully nonlinear numerical simulations of the corresponding Einstein-matter system. We provide evidence that scalar SBSs in the FF are prone to a nonaxisymmetric instability. Thus, such stars are transient states, in a dynamical formation scenario. Assuming an already formed scalar SBS, on the other hand, it collapses into a BH after a nonaxially symmetric instability develops. Vector SBSs (also known as spinning Proca stars), by contrast, are dynamically robust. In the formation scenario we find no evidence of an instability. In agreement, for already formed vector SBSs we observe that (i) even large perturbations are dissipated away, and (ii) some stars in excited families decay to the FF where they remain. This suggests that scalar (vector) SBSs have different dynamical properties and viability, and their toroidal (spheroidal) morphology provides a suggestive interpretation.

SBSs as stationary solutions.—Scalar and vector BSs, with and without spin, arise as equilibrium states in models with Lagrangian density $\mathcal{L} = R/(16\pi G) + \mathcal{L}_m$, where R is the Ricci scalar, G is Newton's constant, and

$$\mathcal{L}_m = -\partial^\alpha \phi \partial_\alpha \bar{\phi} - \mu^2 \phi \bar{\phi}, \quad \mathcal{L}_m = -\frac{\mathcal{F}_{\alpha\beta}\bar{\mathcal{F}}^{\alpha\beta}}{4} - \frac{\mu^2}{2}\mathcal{A}_\alpha \bar{\mathcal{A}}^\alpha \tag{1}$$

describe the scalar and vector cases, respectively. The scalar (ϕ) and vector ($\mathcal{A}_\alpha$) fields are complex valued, with conjugation denoted by an over bar, both with mass μ. As usual, $\mathcal{F} = d\mathcal{A}$. Henceforth, units with $G = 1 = c = \mu$ are used.

Scalar SBSs were first constructed numerically in Refs. [17,18] as asymptotically flat, stationary, and axisymmetric solutions of the above Einstein-Klein-Gordon system. They are a "mass torus" in general relativity; see Fig. 1 (left-hand panel). Scalar SBSs form a discrete set of families of continuous solutions. Each family is labeled by two integers: m, the azimuthal winding number, and n, the node (or overtone) number; see, e.g., Refs. [12,13,19,24,25]. The FF, which has the lowest energy, has $(m, n) = (1, 0)$. Fixing the family, i.e., (m, n), SBSs are characterized by their total mass M and angular momentum J. They form a one-dimensional set, often labeled by M, and oscillation frequency ω. The (dynamically) most interesting solutions occur in between the Newtonian limit, $\omega \to 1$ and $M \to 0$, and the maximal mass solution. The latter occurs for $\omega \to \omega_{M\max}$ ($\simeq 0.775$ for the FF) and the Anowitt-Deser-Misner mass becomes highest, $M \to M_{\max}$ ($\simeq 1.315$ for the FF). In Table I we list the properties of two illustrative scalar SBSs used in the simulations below.

Vector SBSs were first reported as excited states ($n = 1$) in Refs. [6,20]. The FF was considered in Refs. [26,27]. The aforementioned description for scalar SBSs applies, *mutatis mutandis*. An important distinction, however, is that the energy distribution is now spheroidal, rather than toroidal [27]; see Fig. 1 (right-hand panel). Moreover, for the FF, $\omega_{M\max} \simeq 0.562$ and $M_{\max} \simeq 1.125$ [27]. For the excited family with $(m, n) = (1, 1)$, $\omega_{M\max} \simeq 0.839$ and $M_{\max} \simeq 1.568$ [6]. In Table I we list the properties of two (three) representative vector SBSs, in the FF [$(m, n) = (1, 1)$ family].

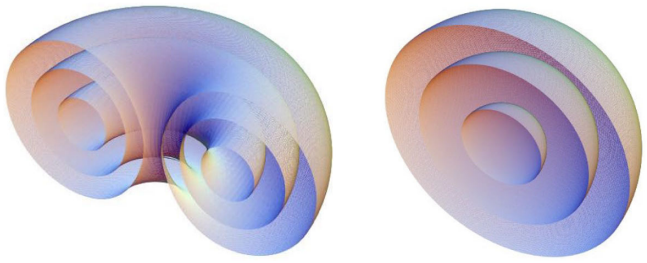

FIG. 1. Surfaces of constant energy density for illustrative SBSs. Left: Scalar configuration 2_S. Right: Vector configuration 1_P. The toroidal vs spheroidal nature is clear.

Dynamical formation of SBSs.—In the spherical case, numerical simulations established that both scalar [7] and vector [8] BSs form dynamically from a spherical "cloud" of dilute scalar or vector field. The cloud collapses due to its self-gravity. The ejection of energetic scalar or vector "particles", dubbed gravitational cooling, allows the formation of a compact object.

For studying the formation of SBSs, with $m = 1$, the Hamiltonian, momentum, and (in the vector case) Gauss constraint are solved by appropriately choosing a Gaussian radial dependence for the key variables, together with a nonspherical profile; see Supplemental Material (SM, Sec. I [28], which includes additional Refs. [29,30]). For the scalar case, the "matter" initial data are

$$\phi(t, r, \theta, \varphi) = Are^{-r^2/\sigma^2} \sin\theta e^{i(\varphi - \omega t)}, \tag{2}$$

where A, σ are constants and $e^{-i\omega t}$ is the harmonic dependence. Besides this unperturbed initial data, we also evolve perturbed initial data of two types: replacing in Eq. (2) $e^{i\varphi} \to e^{i\varphi}[1 + A_1 \cos(2\varphi)]$, or, alternatively, replacing $e^{i\varphi} \to e^{i\varphi} + A_2 e^{2i\varphi}$. A_1, A_2 are the amplitudes of the perturbations.

Fully nonlinear numerical evolutions of the Einstein-matter system using this initial data were carried out with the EINSTEIN TOOLKIT [40,41]; see SM, Sec. II [28], which includes additional Refs. [31–39]. Two choices of A were considered, both of which yield global data for the scalar cloud $(M_{\rm sc}, J_{\rm sc})$ close to that of equilibrium scalar SBS solutions. The first and second choices give $M_{\rm sc}^{(1)} \sim 0.46 \sim J_{\rm sc}^{(1)}$ and $M_{\rm sc}^{(2)} \sim 0.89 \sim J_{\rm sc}^{(2)}$, respectively. We have run simulations with both perturbed and unperturbed initial data, with $A_1 = 0,\ 0.001,\ 0.01,\ 0.05$ and $A_2 = 0,\ 0.05$. Typically, $\sigma = 40$. The evolutions are typically thousands of times longer than the dynamical timescale defined by μ.

All evolutions show the emergence of a nonaxisymmetric instability. The time at which the instability kicks in depends on the type and amplitude of the perturbation, but even the lowest mass unperturbed model ($M_{\rm sc}^{(1)}$) exhibits

TABLE I. Physical properties of some illustrative SBSs. The second row identifies if they are scalar (S) or vector or Proca (P). All solutions have $m = 1$ and none have an ergo region.

Configuration	1_S	2_S	1_P	2_P	3_P	4_P	5_P
Type (S or P)	S	S	P	P	P	P	P
n	0	0	0	0	1	1	1
ω	0.90	0.83	0.95	0.90	0.95	0.90	0.85
M	1.119	1.281	0.534	0.726	1.149	1.456	1.564
J	1.153	1.338	0.543	0.750	1.171	1.500	1.622

nonaxisymmetric features at a sufficiently long timescale [$t \sim \mathcal{O}(10^4)$]. The instability generically triggers a larger ejection of angular momentum than mass, reshaping the toroidal energy distribution into a spherical one. This suggests that the asymptotic end state of the cloud evolution is either a spherical (nonspinning) scalar BS or even, merely, ejected debris carrying all angular momentum and energy.

As an illustration, Fig. 2 exhibits snapshots of the equatorial plane evolution of the energy density ρ_E (left-hand panels) and angular momentum density ρ_J (middle left-hand panels) for the unperturbed scalar initial data with mass $M_{\rm sc}^{(2)}$ [42]. Initially, the collapse preserves axial symmetry. Around $t \sim 4000$, however, the nonaxisymmetric instability is visible, producing a fragmentation event: the star splits into a roughly symmetric orbiting binary. The binary is, nonetheless, bound and recollapses to a deformed spinning star, around $t \sim 6500$. This star breaks into two

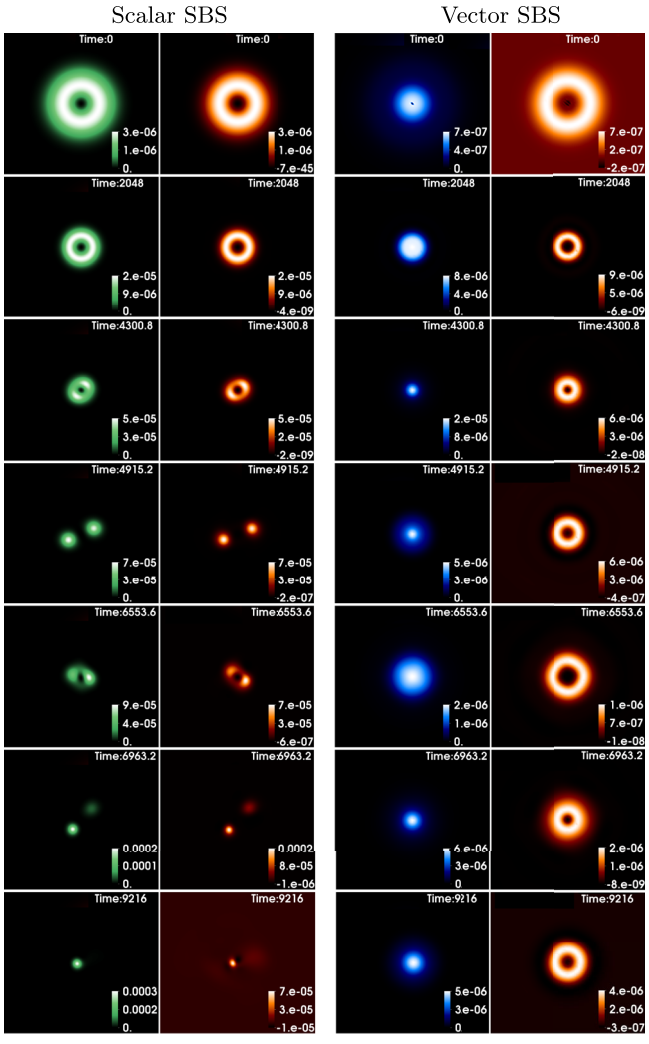

FIG. 2. Time evolution of an equatorial cut of ρ_E (blue or green) and ρ_J (orange) in the formation scenario of a scalar (left-hand side) or a vector (right-hand side) SBS.

asymmetric pieces, which again recollapse into a spheroidal star with angular momentum. Around $t \sim 10\,000$, this residual, still evolving, star has $(M, J) = (0.49, 0.16)$, evaluated up to $r = 30$, and an oscillation frequency $\omega \sim 0.96$. For this ω, the FF static scalar BS has $(M, J) = (0.45, 0)$. Thus, this (or a neighbor) static scalar BS appears to be asymptotically approached, after the remaining J is shed away.

Now consider the formation of a vector SBS. The construction of initial data is more complex due to the Gauss constraint [8,44]. After a $3+1$ splitting of $\mathcal{A}_\mu$, the key variables are the scalar and three-vector potentials together with the electric field. The first of these admits a solution almost identical to Eq. (2), but the others are more involved; see SM, Sec. I [28]. These initial data can again be perturbed. We have considered a perturbation analogous to the first type considered in the scalar case; the perturbation amplitudes studied were $A_1 = A_2 = 0,\ 0.05$. Initial data describing a Proca cloud with three different values of global data were used: $M_{\rm Pc}^{(1)} \sim 0.46 \sim J_{\rm Pc}^{(1)}$, $M_{\rm Pc}^{(2)} \sim 0.56 \sim J_{\rm Pc}^{(2)}$, and $M_{\rm Pc}^{(3)} \sim 0.77 \sim J_{\rm Pc}^{(3)}$.

The unperturbed models' evolutions are instability-free during the simulations, lasting up to $t \sim 10^4$. This is illustrated by the third and fourth columns in Fig. 2, which show snapshots of the time evolution of the unperturbed Proca cloud $M_{\rm Pc}^{(2)}$. The gravitational collapse ejects part of the mass and angular momentum, which shows the gravitational cooling mechanism at play. At $t \sim 10^4$ the star has $(M, J) \sim (0.25, 0.30)$, evaluated up to $r = 30$, and $\omega \sim 0.99$. For this ω, the FF vector SBS has $(M, J) = (0.247, 0.249)$; see SM, Sec. III [28]. Thus, this (or a neighbor) vector SBS appears to be asymptotically approached. For the perturbed initial Proca clouds, on the other hand, the energy density oscillates strongly. Nonetheless, no sudden loss of angular momentum is observed, which suggests the end point is still a vector SBS.

Evolution of equilibrium SBSs.—The dichotomy observed in the formation scenario can be further assessed by considering the dynamics of SBSs obtained as equilibrium solutions of the corresponding Einstein-matter system. A perturbative stability analysis of these SBSs, such as the ones in Refs. [6,9,10] for the spherical case, seems challenging. Thus, we resort to nonlinear numerical evolutions of the Einstein-matter system, analogous to the ones in the formation scenario, but now starting with the equilibrium solutions as initial data. This generalizes the evolutions in Ref. [43] for nonspinning BSs.

We first consider the scalar SBSs. Figure 3 shows the time evolution of model 2_S. Up to $t \sim 1000$ the star remains essentially undisturbed; then, following the development of a nonaxisymmetric perturbation, see upper panels, the star pinches off into two fragments. The resulting binary is gravitationally bound and collapses into a BH at $t \sim 1200$. This is diagnosed by both the appearance of an apparent

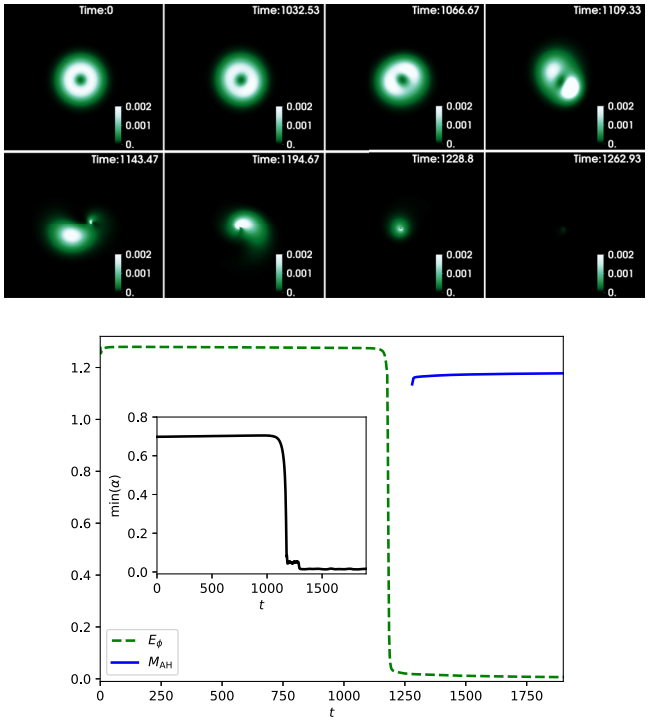

FIG. 3. Time evolution of a scalar SBS, model 2_S. Six sequential snapshots of ρ_E (top panels). Time runs left to right, first to second row. Total scalar field energy and apparent horizon mass (main panel) and lapse function (inset).

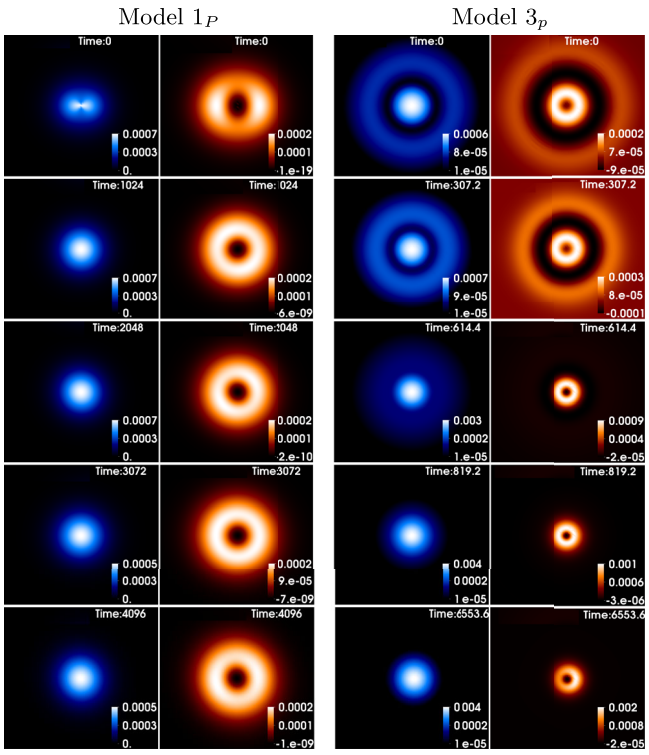

FIG. 4. Time evolution of vector SBSs. Equatorial cut of ρ_E (blue) and ρ_J (orange) for the FF model 1_P with a perturbation (left-hand side) and the excited model 3_P (right-hand side).

horizon, whose mass is shown in the main panel, and the vanishing of the lapse function α, as seen in the inset of Fig. 3. A similar evolution is observed for model 1_S. This confirms that scalar SBSs, even in the FF, are prone to a nonaxisymmetric instability. Unlike the formation scenario, here the instability leads to a complete gravitational collapse, likely due to the more compact initial data.

The behavior of the vector SBSs is distinct. FF solutions, such as models 1_P and 2_P, show no sign of instability, in the absence of large perturbations. They neither disperse away nor collapse to a BH up to $t \sim 4000$, the time at which the drift in the Proca field energy and angular momentum for model 1_P is 2.0% and 2.2%, respectively, whereas for model 2_P, the drift is less than 1%. We further tested the dynamical robustness of vector SBSs by perturbing models 1_P and 2_P and by considering some excited states, such as model $3_P - 5_P$. Figure 4 exhibits the time evolution of two examples: (i) model 1_P with a perturbation of the sort considered in the formation scenario for the vector case, and with a sufficiently large amplitude to visibly distort the star (see first panel), and (ii) the excited model 3_P. In the first case, the perturbation, albeit large enough to deform the morphology of the star away from its spheroidal shape, is dissipated away, and the star recovers its shape. In the second case, the excited state structure of the star is manifest in the composite, Saturn-like, structure of its energy distribution [20]. After $t \sim 1000$, the star abruptly loses energy and angular momentum, until $t \sim 3000$ when it asymptotically tends to a new equilibrium configuration; see SM, Sec. IV [28]. This new configuration has no nodes and it is close to model 2_P. Thus, the star migrates from the excited family to the FF, where it settles, advocating the stability of the latter. Excited models 4_P and 5_P, on the other hand, collapse to a BH.

Interpretation and further remarks.—The contrasting dynamical properties of the scalar or vector SBSs break the phenomenological (qualitative) degeneracy observed between these two types of BSs in the spherical case. It is tempting to attribute this contrast to the different morphology of these stars, as exhibited in Fig. 1. This interpretation is partly supported by the analogy with dynamical instabilities in differentially rotating relativistic (neutron) stars [45]. In that case the existence of a toroidal shape has been suggested to be a necessary condition for the development of nonaxisymmetric corotational instabilities [46,47]. In fact, the pinching instabilities and fragmentation exhibited in the scalar models above are reminiscent of evolutions of unstable toroidal fluid stars [48,49], but also of other corotational instabilities observed in toroidal systems such as the Papaloizou-Pringle instability in accretion disks [50]. Preliminary results, moreover, indicate that vector SBSs with $m = 2$ (which are toroidal) are also unstable. The analogy with corotational instabilities in relativistic fluid stars will be further explored elsewhere.

The instability of scalar SBSs may explain the inability to find them as end points in the evolution of orbiting binaries of (nonspinning) BSs [51,52]. By the same token, however, vector SBSs should form in the equivalent vector scenarios. This suggests revisiting the work in Ref. [16] using constraint-abiding initial data. A related question pertains to the impact of matter self-interactions in the dynamics reported herein.

We thank Carlos Palenzuela, Darío Núñez, Juan Carlos Degollado, and Sergio Gimeno-Soler for useful discussions and valuable comments. This work has been supported by the Spanish Agencia Estatal de Investigacíon (Grants No. AYA2015-66899-C2-1-P and No. PGC2018-095984-B-I00), by the Generalitat Valenciana (ACIF/2015/216, GRISOLIAP/2019/029, PROMETEO/2019/071), by the Fundação para a Ciência e a Tecnologia (FCT) Projects No. PTDC/FIS-OUT/28407/2017, No. UID/MAT/04106/2019 (CIDMA), and No. UID/FIS/00099/2013 (CENTRA), by national funds (OE), through FCT, I. P., in the scope of the framework contract foreseen in the numbers 4, 5, and 6 of the article 23, of the Decree-Law 57/2016, changed by Law 57/2017. This work has further been supported by the European Union's Horizon 2020 research and innovation (RISE) programmes H2020-MSCA-RISE-2015 Grants No. StronGrHEP-690904 and No. H2020-MSCA-RISE-2017, Grant No. FunFiCO-777740. We would like to acknowledge networking support by the COST Action GWverse CA16104. M. Z. acknowledges financial support provided by FCT/Portugal through the IF programme, Grant No. IF/00729/2015. P. C. acknowledges the Ramon y Cajal funding (RYC-2015-19074) supporting his research. Computations have been performed at the Servei d'Informàtica de la Universitat de València, on the "Baltasar Sete-Sois" cluster at IST, and at MareNostrum (via PRACE Tier-0 Grant No. 2016163948).

[1] B. P. Abbott *et al.* (LIGO Scientific Collaboration and Virgo Collaborations), Phys. Rev. X **9**, 031040 (2019).
[2] R. Abuter, A. Amorim, M. Bauböck, J. P. Berger, H. Bonnet, W. Brand ner, Y. Clénet, V. Coudé Du Foresto, and P. T. de Zeeuw (Gravity Collaboration), Astron. Astrophys. **618**, L10 (2018).
[3] K. Akiyama *et al.* (Event Horizon Telescope), Astrophys. J. **875**, L1 (2019).
[4] D. J. Kaup, Phys. Rev. **172**, 1331 (1968).
[5] R. Ruffini and S. Bonazzola, Phys. Rev. **187**, 1767 (1969).
[6] R. Brito, V. Cardoso, C. A. R. Herdeiro, and E. Radu, Phys. Lett. B **752**, 291 (2016).
[7] E. Seidel and W.-M. Suen, Phys. Rev. Lett. **72**, 2516 (1994).
[8] F. Di Giovanni, N. Sanchis-Gual, C. A. R. Herdeiro, and J. A. Font, Phys. Rev. D **98**, 064044 (2018).
[9] M. Gleiser and R. Watkins, Nucl. Phys. **B319**, 733 (1989).
[10] T. D. Lee and Y. Pang, Nucl. Phys. **B315**, 477 (1989).
[11] N. Sanchis-Gual, C. Herdeiro, E. Radu, J. C. Degollado, and J. A. Font, Phys. Rev. D **95**, 104028 (2017).
[12] F. E. Schunck and E. W. Mielke, Classical Quantum Gravity **20**, R301 (2003).
[13] S. L. Liebling and C. Palenzuela, Living Rev. Relativity **15**, 6 (2012); **20**, 5 (2017).
[14] C. Palenzuela, I. Olabarrieta, L. Lehner, and S. L. Liebling, Phys. Rev. D **75**, 064005 (2007).
[15] C. Palenzuela, L. Lehner, and S. L. Liebling, Phys. Rev. D **77**, 044036 (2008).
[16] N. Sanchis-Gual, C. Herdeiro, J. A. Font, E. Radu, and F. Di Giovanni, Phys. Rev. D **99**, 024017 (2019).
[17] F. E. Schunck and E. W. Mielke, Phys. Lett. A **249**, 389 (1998).
[18] S. Yoshida and Y. Eriguchi, Phys. Rev. D **56**, 762 (1997).
[19] B. Kleihaus, J. Kunz, M. List, and I. Schaffer, Phys. Rev. D **77**, 064025 (2008).
[20] C. Herdeiro, E. Radu, and H. Runarsson, Classical Quantum Gravity **33**, 154001 (2016).
[21] F. H. Vincent, Z. Meliani, P. Grandclement, E. Gourgoulhon, and O. Straub, Classical Quantum Gravity **33**, 105015 (2016).
[22] Z. Meliani, F. H. Vincent, P. Grandclément, E. Gourgoulhon, R. Monceau-Baroux, and O. Straub, Classical Quantum Gravity **32**, 235022 (2015).
[23] C. A. R. Herdeiro and E. Radu, Phys. Rev. Lett. **112**, 221101 (2014).
[24] P. Grandclement, C. Somé, and E. Gourgoulhon, Phys. Rev. D **90**, 024068 (2014).
[25] C. Herdeiro and E. Radu, Classical Quantum Gravity **32**, 144001 (2015).
[26] C. A. R. Herdeiro and E. Radu, Phys. Rev. Lett. **119**, 261101 (2017).
[27] C. Herdeiro, I. Perapechka, E. Radu, and Ya. Shnir, Phys. Lett. B **797**, 134845 (2019).
[28] See Supplemental Material at http://link.aps.org/supplemental/10.1103/PhysRevLett.123.221101 for further details on the initial data, code assessment and profiles and evolutions of physical quantities, which includes Refs. [29–39].
[29] I. Cordero-Carrion, P. Cerda-Duran, H. Dimmelmeier, J. L. Jaramillo, J. Novak, and E. Gourgoulhon, Phys. Rev. D **79**, 024017 (2009).
[30] H. Okawa, H. Witek, and V. Cardoso, Phys. Rev. D **89**, 104032 (2014).
[31] F. Loffler, J. Faber, E. Bentivegna, T. Bode, P. Diener *et al.*, Classical Quantum Gravity **29**, 115001 (2012).
[32] M. Zilhão and F. Löffler, Int. J. Mod. Phys. A **28**, 1340014 (2013).
[33] E. Schnetter, S. H. Hawley, and I. Hawke, Classical Quantum Gravity **21**, 1465 (2004).
[34] Carpet: Adaptive mesh refinement for the cactus framework, http://www.carpetcode.org/.
[35] J. Thornburg, Classical Quantum Gravity **21**, 743 (2004).
[36] J. Thornburg, Phys. Rev. D **54**, 4899 (1996).
[37] H. Witek and M. Zilhão, CANUDA, https://bitbucket.org/canuda/.
[38] U. Sperhake, Phys. Rev. D **76**, 104015 (2007).
[39] D. Brown, P. Diener, O. Sarbach, E. Schnetter, and M. Tiglio, Phys. Rev. D **79**, 044023 (2009).
[40] EinsteinToolkit, Einstein Toolkit: Open Software for Relativistic Astrophysics, http://einsteintoolkit.org/.
[41] F. Löffler, Classical Quantum Gravity **29**, 115001 (2012).
[42] The energy and angular momentum densities are the ones defined from the Komar integrals, as in Refs. [16,43].

[43] P. V. P. Cunha, J. A. Font, C. Herdeiro, E. Radu, N. Sanchis-Gual, and M. Zilhão, Phys. Rev. D **96**, 104040 (2017).
[44] M. Zilhão, H. Witek, and V. Cardoso, Classical Quantum Gravity **32**, 234003 (2015).
[45] V. Paschalidis and N. Stergioulas, Living Rev. Relativity **20**, 7 (2017).
[46] M. Saijo, T. W. Baumgarte, and S. L. Shapiro, Astrophys. J. **595**, 352 (2003).
[47] A. L. Watts, N. Andersson, and D. I. Jones, Astrophys. J. **618**, L37 (2005).
[48] B. Zink, N. Stergioulas, I. Hawke, C. D. Ott, E. Schnetter, and E. Mueller, Phys. Rev. Lett. **96**, 161101 (2006).
[49] B. Zink, N. Stergioulas, I. Hawke, C. D. Ott, E. Schnetter, and E. Mueller, Phys. Rev. D **76**, 024019 (2007).
[50] K. Kiuchi, M. Shibata, P. J. Montero, and J. A. Font, Phys. Rev. Lett. **106**, 251102 (2011).
[51] M. Bezares, C. Palenzuela, and C. Bona, Phys. Rev. D **95**, 124005 (2017).
[52] C. Palenzuela, P. Pani, M. Bezares, V. Cardoso, L. Lehner, and S. Liebling, Phys. Rev. D **96**, 104058 (2017).